SOCIETY OF AUTOMOTIVE ENGINEERS, INC.
Two Pennsylvania Plaza, New York, N.Y. 10001

LOW-SPEED AERODYNAMIC CHARACTERISTICS OF A

13.1-PERCENT-THICK, HIGH-LIST AIRFOIL

Kenneth R. Sivier, Allen I. Ormsbee, and Randal W. Awker
Aeronautical and Astronautical Engineering Department
University of Illinois

SOCIETY OF AUTOMOTIVE ENGINEERS

Business Aircraft Meeting
Wichita, Kans.   740366
April 2—5, 1974

LOW-SPEED AERODYNAMIC CHARACTERISTICS OF A

13.1-PERCENT-THICK, HIGH-LIFT AIRFOIL*

by

Kenneth R. Sivier, Allen I. Ormsbee, and Randal W. Awker
Aeronautical and Astronautical Engineering Department
University of Illinois
Urbana-Champaign Campus

ABSTRACT

This paper is concerned with the experimental study of the low-speed, sectional characteristics of a high-lift airfoil and the comparison of those characteristics with the predictions of the theoretical methods used in the airfoil's design. The 13.1-percent-thick, UI-1720 airfoil was found to achieve the predicted maximum lift coefficient of nearly 2.0. No upper-surface, flow separation was found below the stall angle of attack of 16 degrees; it appeared that stall was due to an abrupt leading-edge flow separation.

1. INTRODUCTION

For the past several years, a group at the University of Illinois has been involved in the study of analytical methods suitable for the design of high-lift airfoils (1,2,3), an activity being pursued by a number of other investigators (4,5,6) as well. The airfoils are characterized generally by combining high maximum lift with low drag, resulting in high lift-to-drag ratios.

The work reported here represents the first effort to evaluate experimentally, an airfoil designed by the methods used at the University of Illinois (2,3). The airfoil studied was the 13.1-percent-thick UI-1720, an optimized design that, theoretically, achieves a sectional lift coefficient of 2.0 at an angle of attack of 11.7 degrees and a Reynolds number of 1.75×10^6. Since this testing program was the first to be conducted in the University of Illinois 10-by-60-inch, two-dimensional, low-speed wind tunnel, a considerable part of the program was involved in determining that the test results were valid.

2. THEORETICAL BACKGROUND

The UI-1720 airfoil was designed (3) by a two-step process. In the first step, an optimization procedure (2) was used to determine the upper-surface pressure distribution necessary to give a maximum lift coefficient at a given design Reynolds number. The general characteristics of the upper surface pressure distribution are: (1) a constant pressure segment (rooftop) from the leading edge aft to some chordwise location X_o, and (2) a pressure recovery segment from X_o aft to the trailing edge. The maximum lift requirement has been shown (2) to require that the pressure recovery be the largest possible. To achieve this, a modification of an expression derived by Stratford (7,2) was used to obtain a pressure gradient that maintained zero skin friction (incipient separation) along the pressure recovery segment.

The lower-surface pressure distribution was not determined at this stage. Instead, it was allowed to "float". The distribution was determined later by satisfying the condition that the airfoil section be closed at the trailing edge.

The second step in the design process was to apply an inverse conformal mapping method developed by Eppler (8) and modified by Miley (9). Through an iterative application of this method, an airfoil contour (which includes the angle of attack), corresponding to the given pressure distribution, was found. In the design of the UI-1720 airfoil, a pressure recovery gradient slightly less than the maximum possible was selected as a safeguard against early stall in the test program.

The pressure distributions obtained from the Eppler/Miley theory are for potential flow only. To obtain viscous-flow pressure distributions for comparison with experimental data, a computerized method, developed by the Lockheed Georgia Company for NASA (10), was used.

The UI-1720 airfoil was designed to give a maximum lift coefficient of 2.0 (predicted by potential flow) at a Reynolds number of 1.75×10^6 with a turbulent boundary layer over the entire upper surface. The theory predicts that the design lift coefficient will be achieved at an angle of attack of 11.68 degrees. Figure 1 shows the UI-1720 contour and lists the coordinates for this 13.1-percent-thick airfoil. Figure 2 presents a comparison of the Eppler and Lockheed pressure distributions at the design angle of attack. The major difference occurs near the leading edge on the upper surface where the more positive pressure predicted by the Lockheed program should result in decreased lift and increased pressure drag.

Finally, Figure 3 presents the integrated sectional coefficients for the design Reynolds number. In each case, the total drag coefficient was obtained through the application of the Squire-Young relation (9) at the trailing edge.

3. APPARATUS

3.1 Wind Tunnel Facility

The experimental studies were carried out in the 10-by-60-inch, two-dimensional test section of the University of Illinois low-speed wind tunnel. Figure 4 presents a sketch of the tunnel layout. The tunnel is of the open-return type with the fan at the inlet. A honeycomb and three screens are located at the inlet to the settling section to control flow uniformity and turbulence. The diffuser has an included angle of about 8 degrees and an area ratio of 3.1; this geometry was determined empirically to maximize pressure recovery, while retaining steady flow and only mild separation in the diffuser.

The tunnel has a maximum empty test-section speed of about 250 ft/sec. The fan is driven by a constant-speed a.c. motor; tunnel speed control is obtained by manual adjustment of the pitch of the fan blades.

As shown in Figure 5, the test-section reference conditions are measured at a point three inches downstream of the test-section entrance

and 10 inches above the centerline. The static pressures are obtained from orifices in each sidewall and the total pressures by probes located three inches from each wall.

For the studies reported here, a wake rake was located on a vertical strut downstream of the model location, Figure 5. The vertical location of the rake could be controlled remotely with an accuracy better than ± 0.005 inches. A photograph and a layout sketch of the rake are presented in Figure 6. The rake's orientation was horizontal (i.e., parallel to the model span) permitting simultaneous wake surveys at 10 spanwise locations. The two end probes were located one-half inch from their respective side-walls and hence were within the sidewall boundary layers. Note that this rake could not be pitched and hence the probes were at all times parallel to the test section centerline. The probe orifices were located 5.9 inches (0.39 chord lengths) downstream of the model trailing edge.

3.2 Airfoil Model Assembly

The model assembly consisted of the airfoil proper together with attached end-plates (see Figure 7). The end-plate diameters were unequal and such that the model assembly could be "plugged" easily into the test section from one side.

The model itself had a span of 10 inches, a nominal chord of 15 inches, and a thickness of 1.965 inches. It was machined from two pieces of aluminum, one forming a removable lower surface, making it possible to instrument the model from the inside, see Figure 7. The rough machining, instrumentation, and mating to the end-plates were done at the University of Illinois, while the surface contour machining was done at the NASA Langley Research Center. Table I presents a listing of the as-machined coordinates. Due to a machining error, the model chord was slightly less than the nominal 15 inches. As a result, the as-machined coordinates differ slightly from the theoretical values; but they are correct for the shortened chord. All theoretical results were based on these coordinates.

The model was instrumented by 65, 0.050-inch surface pressure taps, of which 34 were distributed along the model centerline. The coordinates of the pressure taps are listed in Table 2. Note that four rows of spanwise taps were included to aid in evaluating the two-dimensionality of the flow over the airfoil.

3.3 Sidewall Blowing System

One of the major problems in two-dimensional airfoil testing involves the interaction of the sidewall boundary layer with the model flow field. In particular, the sidewall boundary layer tends to separate in regions of adverse pressure gradient generated by the airfoil. A standard way of controlling this separation is to introduce sidewall blowing or suction in regions where the possibility of separation is greatest. Because blowing systems have been found more effective and less critical to design and operate (11,12) and because of the availability of high pressure air, a blowing system was selected for the University of Illinois two-dimensional wind tunnel.

Figure 8 shows the configuration of the blowing slot assembly. Each slot was 3 inches long and began just below the model surface. Figure 7a shows the slots installed in the endplates. The chordwise position of the blowing slots was chosen to be slightly upstream of the start of the design pressure recovery at the 16.2% c position. While the blowing coefficient could be changed either by changing the blowing slot width or varying the supply pressure, it was found that the latter method was the more convenient procedure.

3.4 Instrumentation

The most negative model surface pressures were measured by use of a manually-operated pressure scanning system made up of a 48-position Scani-valve and a 5 psig strain-gauge pressure transducer. The read-out was done manually with a digital millivoltmeter. The remaining model surface pressures, together with the wake rake and tunnel reference pressures, were measured on a multi-tubed oil manometer. The blowing supply pressure was measured by a high-precision bourdon-tube pressure gauge. The angle of attack was set by reference to angles scribed on the plexiglass endplate.

4. EXPERIMENTAL RESULTS

4.1 Test Conditions

The experimental data were obtained at nominal test-section speeds of 190 and 250 fps, corresponding to Reynolds number of 1.4×10^6 and 1.8×10^6, respectively. Unless otherwise noted, the data were obtained with the

wake rake assembly in place and with sidewall blowing supply pressures of
about 16 psig. The angle of attack range was from - 4 degrees (approxi-
mately the zero-lift angle) to stall. Finally, unless otherwise noted, the
data were for a clean airfoil leading edge.

4.2 Data Reductions and Corrections

All data reduction was handled by computer programs that, in the case
of the wing surface pressures, reduced the measured pressures to pressure
coefficient form, i.e.,

$$c_p = \frac{p - p_\infty}{q_\infty}$$

The resulting pressure coefficient distributions then were integrated
numerically to obtain values of the normal force, chord force, and leading-
edge pitching moment coefficients. These, in turn, were resolved to give
the sectional values of lift and quarter-chord pitching moment coefficient.

The sectional drag coefficients were obtained from the wake pressure
data through the relation (13)

$$c_d = 2 \int \left(\sqrt{\frac{q}{q_o}} - \frac{q}{q_o} \right) \frac{dy}{c}$$

where, because of an approximately 3-percent change in the local reference
dynamic pressure across the wake, q_o was taken as the linearly interpolated
value between the free-stream values immediately above and below the wake.

Tunnel empty measurements showed that the static pressure at the test
section center was approximately 2.6 percent smaller than the measured
reference static pressure, p_{ref}; the total pressure did not vary. In addi-
tion, it was found that the model itself affected the p_{ref} measurement, the
extent of the effect varying with the model angle of attack. To correct the
measured p_{ref} and q_{ref} to the tunnel empty, test-section center value, the
following procedure was used;

$$q_\infty = q_{ref} (1 + \Delta q_{model})(1 + \Delta q_o)$$

$$p_\infty = p_{ref} - (q_\infty - q_{ref})$$

where

$$\Delta q_{model} = \frac{(q_{ref})_{model\ out} - (q_{ref})_{model\ in}}{(q_{ref})_{model\ in}}$$

and

$$\Delta q_o = 0.026$$

These values, p_∞ and q_∞, were taken as the undisturbed free-stream values for the test. The magnitude of these corrections varied from a decrease in reference dynamic pressure of 2.5 percent near stall to an increase of about 4.0 percent at -4 degrees angle of attack.

The uncorrected values of the pressure, lift, drag, and moment coefficients were based on q_∞. No further correction was applied to the pressure coefficients. However, the angle of attack, dynamic pressure (and hence reference airspeed and Reynolds number), and the lift, drag, and moment coefficients were corrected additionally for tunnel boundary effects using the standard two-dimensional corrections (13). The magnitude of the boundary corrections is indicated in Figure 9, which presents a comparison of uncorrected and corrected sectional data for the $Re = 1.8 \times 10^6$ case.

4.3 Validity of the Data

One of the major concerns in a two-dimensional wind tunnel test program is whether or not the resulting data are truly two-dimensional. This was an especially important point in the subject program because of the small aspect ratio (0.67) of the model. The spanwise variation of the surface pressure data represents one check of flow two-dimensionality. Figures 10 and 11 present typical examples of spanwise data. Figure 10 shows data obtained from the four spanwise rows of pressure taps. While the downstream locations show good to excellent uniformity, the most upstream location shows a substantial pressure increase toward the wall. It should be noted, however, that the taps nearest the wall are within the wall boundary layer and that the most upstream location is well upstream of the blowing slot.

In Figure 11, pressure distributions from the model centerline and wall line are compared. Considering that the wall taps lie within the wall boundary layer, the agreement is excellent. Only on the upper surface, near

the leading edge (and forward of the blowing slot) do the wall pressures vary significantly from the centerline values.

Another indicator of two-dimensionality is the spanwise variation of the wake characteristics, including the sectional drag. Figure 12 presents a typical carpet plot of the dynamic pressure distribution through the wake. The curve labeled 1, corresponding to the total pressure tube closest to the aluminum end plate, was plotted at its calculated values. For each succeeding curve, the origin was shifted + 0.25 psi. All of the distributions are qualitatively similar and only near the walls does the static pressure variation, transverse to the wake, appear significant. Note also that the wake moves downward as the walls are approached, suggesting the possibility of downwash effects and, hence, an imperfection in the two-dimensionality of the flow.

Figure 13 shows the sectional drag coefficient data for several angles of attack, including the one corresponding to the data of Figure 12. Again, the deviation from a uniform c_d - distribution is greatest as the walls are approached and at the highest angles of attack. However, fair uniformity appears present over the portion of the span covered by the central six probes, even at the highest angles of attack.

Two flow visualization techniques were employed to check further on the two-dimensionality of the flow. In the first, yarn tufts were applied to the airfoil's upper surface and to the aluminum end plate. These tufts indicated smooth, steady flow (with no regions of separated flow, secondary flow, or vortex flow) at all angles of attack up to the stall, when the flow became very unsteady.

A naphthalene evaporation technique (discussed more fully in Section 4.4) was used to detect the laminar-to-turbulent boundary layer transition. Except for local disturbances due to the pressure tap holes, the transition line was observed to be sharp and in the spanwise direction. This then was another indicator that the flow was two-dimensional.

As discussed in Section 3.3, control of the sidewall boundary layer separation was achieved by blowing slots located in the endplates just upstream of the onset of pressure recovery on the airfoil's upper surface. A series of tests at blowing pressures from 0 to 30 psig (all at a fixed slot opening of 0.011 inches) showed that with no blowing and with blowing pressures exceeding 30 psig, the airfoil stalled early. For blowing pressures

between 0.3 and 30 psig, the stall angle of attack was constant and only minor changes in the pressure distributions and sectional coefficients occurred. This result, while not a definite indicator of two-dimensional flow, strongly suggests the absence of sidewall boundary separation effects when compared with results obtained by other investigators (11,12). For the remainder of the data reported here, a blowing pressure of 16 psig and a slot opening of 0.011 inch was arbitrarily selected. These values gave a blowing momentum coefficient

$$c_\mu = \frac{\dot{m}V_j}{q_\infty C}$$

of about 0.04, a value within the range of c_μ found by van den Berg (12) to yield acceptable two-dimensional flow.

One final point needs to be reviewed in a consideration of the validity of the test results. The wake rake used in these investigations was located about one-half chord length behind the model. As can be seen in Figure 6, the rake must act as a large airfoil, always at zero angle of attack, in wake of the test airfoil. Further, the probe orifices are not very far (in, say, body diameters) forward of the pod that holds the rake head. Two situations must be considered here. First, does the presence of the rake affect the airfoil flow? This effect is shown in Figure 14, in which rake-out data are compared with the rake-in data (which will be discussed in Section 4.4). These data show that the wake effect, on lift and pitching moment, is negligible.

The second possible rake effect arises because the rake angle remained fixed, independent of the airfoil angle of attack. With the probe orifices close to the model trailing edge (about 1/3 chord length), it is likely that the wake flow still has some angularity. This conclusion is further substantiated by the free-stream dynamic pressure change, of about 3-percent, across the wake. Such a change can be caused only by a static pressure change and the static pressure change indicates that the streamlines are still curved. With this situation, the static pressure probes will indicate an erroneous pressure due to their angle of attack. If the indicated static pressure is smaller than actual (this would be the expected result for a static pressure probe at angle of attack (14)), the corresponding dynamic pressure will be greater than actual, since the total pressure probes are insensitive to small angles of attack. This effect will occur both outside and inside the

wake. However, the error in dynamic pressure will be greater within the wake, so that the net result will be an indicated drag less than actual. It appears, therefore, that the measured profile drag may be optimistic at the higher angles of attack.

4.4 Discussion of Results

Figures 15 and 16 present typical centerline surface pressure distributions for Reynolds numbers of 1.8×10^6 (the design value) and 1.4×10^6, respectively. Also included, for comparison, are the corresponding pressure distributions calculated using the Lockheed program (10) (using the as-machined model coordinates). The generally excellent agreement between experiment and theory at low angles of attack, deteriorates at the higher angles. The differences are most pronounced on the upper surface, especially near the leading edge. Note, however, that no evidence of upper surface flow separation appears, even at the highest angles of attack. As observed by others (6), the Lockheed program over-predicts the negative pressures near the leading edge at the higher angles of attack. Note that, at 15 degrees (Figure 15d), the predicted pressure coefficient spike has not appeared in the experimental data. However, at 16 degrees (Figure 16b), the spike is very prominent. Comparing Figures 15d and 16b, it is seen that the spike is growing very rapidly with angle of attack. This observation suggests that stall, which experimentally was found to occur just above 16 degrees, occurs due to separation at the leading edge and hence occurs as an abrupt rather than gradual process.

Figure 15c illustrates the effectiveness of the Eppler and Lockheed programs in predicting the starting point and rate of the pressure recovery on the upper surface. The Eppler design program predicted the starting point at 19.6% c. The Lockheed program predicted a value of 19.0% c, while the experiment shows the start at about 18.5% c, at the design angle of attack. The theoretical pressure recovery rate also agrees very well with the experiment.

Figure 17 presents a comparison of the pressure coefficient distribution for the design angle of attack and the two test Reynolds numbers. The experimental and theoretical data both show slightly more negative pressures, at the higher Reynolds number, over the forward part of the upper surface. This effect is not apparent at the zero-lift condition and grows as the angle of attack is increas d.

Figure 18 presents the integrated airfoil sectional characteristics, again compared with the results predicted by the Lockheed program. The lift coefficient data show that the Lockheed program overpredicts the lift curve slope. The experimental data fall just below the thin-airfoil result of 2π per radian. Reference to the pressure distribution data in Figures 15 and 16 shows that the lift deficiency arises primarily due to the more positive pressures found on the upper surface near the leading edge. These more positive pressures must be, at least, an important part of the reason for the increased drag (compared with the theoretical values) at the higher angles of attack.

The reason for the difference in pitching moments is less clear. In this case, the more positive pressures near the leading edge should produce a negative change in moment from the theoretical result. Just the opposite is observed. Most of the Re = 1.4×10^6, rake-in data were taken early in the program when the model contained too few pressure taps for good pressure distribution definition near the leading edge. While not affecting the lift data to a significant degree, this situation yielded some poor pitching moment data. The rake-out data have been included to improve the definition of the pitching moment at the lower Reynolds number. All of the Re = 1.8×10^6 data were taken after more pressure taps were added to the model.

Reynolds number effects appear in all three coefficients and the effects are qualitatively as predicted by the Lockheed program results. The lift-coefficient effect corresponds directly to the difference in rooftop pressures shown in Figure 17. These more negative pressures at the higher Reynolds number also probably cause the drag and pitching moment changes shown.

The lift-to-drag ratio data are presented in Figure 19. These data show a maximum value of c_ℓ/c_d of about 106 for R_e = 1.8×10^6; insufficient data are available to establish a comparative value for the lower Reynolds number.

In an effort to determine whether the model boundary layer was laminar or turbulent, a naphthalene evaporation method was used. The naphthalene was dissolved in petroleum ether and the resulting solution was sprayed onto the wing's upper surface, forming a thin layer of naphthalene. With the wind tunnel running, the naphthalene evaporated at different rates depending

on whether the flow was laminar or turbulent, giving a visual indication of what was happening in the boundary layer. This technique showed a sharp line at the approximate location of the start of the pressure recovery (i.e., the naphthalene evaporated faster downstream of this line), indicating a boundary layer transition at this point. The line was observed for both Reynolds numbers and with or without sidewall blowing. Thus, it appears that the boundary layer was laminar on the upper surface forward of the point at which the pressure recovery began. However, it also was noticed that the static pressure taps apparently were tripping the boundary layer locally, suggesting that the flow over all the centerline pressure taps was turbulent at all test conditions.

An attempt was made to trip the boundary layer by roughening the leading edge. This was done by roughening a thin coat of rubber cement after curing; any greater roughness than this caused premature stall. This resulted in the disappearance of the line in the naphthalene at the pressure recovery point, indicating that the flow on the entire upper surface was turbulent. Effects due to roughness did not appear in the lift and pitching moment coefficients. As shown in Figure 20, a small increase in drag coefficient appeared at 8 degrees angle of attack, but insufficient data are available to establish this effect with certainty.

5. CONCLUSIONS

The objectives of the subject study were to determine, experimentally, the low-speed sectional characteristics of a high-lift airfoil and to compare those characteristics with those predicted by the theoretical methods used in designing the airfoil. A secondary objective was to evaluate the performance of the University of Illinois, 10-by-60-inch, two-dimensional wind tunnel.

The airfoil studied was the UI-1720, designed to achieve a lift coefficient of 2.0 at an angle of attack of 11.68 degrees and a Reynolds number of 1.75×10^6. The following conclusions can be drawn from this study.

    1. The design procedure (combining the Ormsbee-Chen optimization technique with the modified Eppler inverse mapping method) was successful in designing an airfoil having a maximum sectional lift coefficient of about 2.0 with no flow separation up to the stalling angle of attack. However, the maximum lift coefficient occurred

experimentally at an angle of attack of about 16 degrees rather than the predicted value of 11.7 degrees. The zero-lift angle of attack (found to be about - 4.6 degrees) agreed with the value predicted by the Lockheed program.

2. While the lift performance prediction was good (although the experimental lift-curve slope fell below the predicted value), the pitching moment and drag coefficient predictions were less accurate. The pitching moment coefficient was found to be less negative (than either the Eppler or Lockheed program values), at the zero-lift condition, and became even less negative as the angle of attack increased. The latter result indicated that the aerodynamic center moved forward with increasing angle of attack.

3. The zero-lift drag was found to be less than that predicted by the Lockheed program, but increased with increased lift. The Lockheed program prediction of decreased drag coefficients at high lift coefficients, raises a serious question about its ability to predict airfoil drag.

4. The Lockheed program predicted the surface pressure distribution very well except on the upper surface near the leading edge; the experimental values were found to be much more positive.

5. No upper surface separation was found at any angle below the stall. However, as the stalling angle was approached, a significant negative pressure spike, followed by a steep pressure recovery, was observed at the leading edge. This suggested that the observed abrupt stall was caused by leading-edge flow separation.

6. The experimental spanwise variation in the airfoil characteristics indicated that valid two-dimensional studies can be carried out, at least up to a lift coefficient of 2, in the University of Illinois two-dimensional tunnel. The usual tunnel boundary corrections were found to be small, as should be expected for a tunnel-height-to-wing-chord ratio of 4. Modest sidewall blowing

was found to control sidewall boundary layer separation and its
effect on the two-dimensionality of the flow.

6. REFERENCES

1. Liebeck, R. H. and Ormsbee, A. I., "Optimization of Airfoils for
   Maximum Lift", Journal of Aircraft, Vol. 7, No. 5, September-
   October 1970, pp 409-415.

2. Ormsbee, A. I. and Chen, A. W., "Multiple Element Airfoils Optimized
   for Maximum Lift Coefficient", Journal of Aircraft, Vol. 10, No. 12,
   December 1972, pp 1620-1624.

3. Awker, R. W., "The Design and Test of a Single Element Airfoil
   Optimized for High Lift", Master's Thesis, University of Illinois,
   March 1974.

4. Liebeck, R. H., "A Class of Airfoils Designed for High Lift in Incom-
   pressible Flow", Journal of Aircraft, Vol. 10, No. 10, October 1973,
   pp 610-617.

5. Bingham, G. J. and Chen, A. I., "Low-Speed Aerodynamic Characteristics
   of an Airfoil Optimized for Maximum Lift Coefficient", NASA TN
   D-7071, 1972.

6. McGee, R. J. and Beasley, W. D., "Low-Speed Aerodynamic Characteristics
   of a 17-Percent-Thick Airfoil Section Designed for General Aviation
   Applications", NASA TN D-7428, 1973.

7. Stratford, B. S., "The Prediction of Separation of the Turbulent
   Boundary Layer", Journal of Fluid Mechanics, Vol. 5, 1959.

8. Eppler, R., "Ergebnisse gemeinsamer Anwendung von Grenzschicht-und
   Profiltheorie", Zeitshrift fur Flugwissenshaften, September 1960.

9. Miley, S. J., "An Analysis of the Design of Airfoil Sections for Low
   Reynolds Numbers", Ph.D. Thesis, Mississippi State College, 1972.

10. Stevens, W. A., Goradia, S. H., and Braden, J. A., "Mathematical Model
    for Two-Dimensional, Multi-Component Airfoils in Viscous Flow",
    NASA CR-1843, July 1971.

11. Englar, R. J. and Williams, R. M., "Test Techniques for High Lift, Two-
    Dimensional Airfoils with Boundary Layer and Circulation Control for
    Application to Rotary Wing Aircraft", presented at the Canadian
    Aeronautics and Space Institute Annual General Meeting, May 1972.

12. van den Berg, B., "Some Notes on Two-Dimensional High-Lift Tests in
    Wind-Tunnels", AGARD Lecture Series No. 43, Lecture No. 5, February
    1971.

13. Pope, A. and Harper, J. J., <u>Low-Speed Wind Tunnel Testing</u>, John Wiley
     and Sons, Inc., 1966.

14. Ower, E. and Pankhurst, R. C., <u>The Measurement of Air Flow</u>, Pergamon
     Press Ltd., 1966.

TABLE 1

MACHINED COORDINATES OF THE UI 1720-00

NOTE: THE ORIGIN IS AT THE LEADING EDGE

X	Y	X	Y
0.999999	0.000954	0.008823	0.024374
0.996716	0.002736	0.004278	0.016285
0.991189	0.004605	0.001315	0.008783
0.983287	0.006601	0.0	0.0
0.973009	0.008816	0.000641	-0.004765
0.960402	0.011253	0.003744	-0.010051
0.945505	0.013875	0.009317	-0.015090
0.928386	0.016725	0.016852	-0.019595
0.909105	0.019755	0.026156	-0.023426
0.887774	0.022946	0.037148	-0.026336
0.864469	0.026323	0.050349	-0.027964
0.839327	0.029913	0.066134	-0.028652
0.812464	0.033731	0.084314	-0.028739
0.784032	0.037709	0.104783	-0.028238
0.754179	0.041927	0.127428	-0.027264
0.723085	0.046265	0.152142	-0.025869
0.690895	0.050763	0.178825	-0.024080
0.657818	0.055368	0.207351	-0.021964
0.624014	0.060074	0.237571	-0.019588
0.589703	0.064859	0.269333	-0.017032
0.555064	0.069731	0.302510	-0.014343
0.520305	0.074650	0.336888	-0.011606
0.485627	0.079562	0.372308	-0.008850
0.451242	0.084460	0.408554	-0.006147
0.417351	0.089273	0.445456	-0.003531
0.384161	0.093938	0.482784	-0.001121
0.351885	0.098396	0.520319	0.001121
0.320743	0.102581	0.557841	0.003117
0.290930	0.106398	0.595155	0.004825
0.262692	0.109755	0.632003	0.006280
0.236269	0.112518	0.668183	0.007402
0.211962	0.114427	0.703456	0.008209
0.190065	0.114861	0.737634	0.008670
0.169782	0.112966	0.770477	0.008696
0.150220	0.109141	0.801785	0.008590
0.131513	0.104303	0.831385	0.008222
0.113747	0.098496	0.859062	0.007608
0.097028	0.091809	0.884651	0.006794
0.081417	0.084347	0.908004	0.005800
0.067001	0.076378	0.928974	0.004725
0.053853	0.068029	0.947394	0.003637
0.042013	0.059526	0.963198	0.002536
0.031535	0.050676	0.976253	0.001635
0.022485	0.041600	0.986498	0.00 008
0.014903	0.032750	0.994139	0.C 0574
		0. 9232	0.000340

TABLE 2. PRESSURE TAP LOCATIONS

	UPPER SURFACE				LOWER SURFACE	
	x	x/c			x	x/c
	13.625"	0.909		*	0.031	0.002
S	9.00	0.60			0.125	0.008
	7.00	0.47			0.562	0.04
	5.50	0.37		*	0.812	0.05
	4.750	0.32		*	1.250	0.08
	4.250	0.28		*	2.000	0.13
S	3.750	0.25		*	2.500	0.17
	3.250	0.22			3.500	0.23
	3.000	0.20		*	5.000	0.33
	2.875	0.19		*	6.500	0.43
S	2.594	0.17			8.000	0.53
*	2.250	0.15			13.625	0.909
	2.000	0.13				
*	1.750	0.12				
*	1.375	0.09				
S	1.000	0.07				
*	0.750	0.05				
*	0.625	0.04				
	0.375	0.03				
*	0.200	0.01				
*	0.062	0.004				
*	0.000	0				

S Indicates spanwise row of taps.

* Indicates taps on both center and wall lines.

UI-1720 Airfoil Coordinates for c = 15 Inches

Upper Surface

x, inches	y, inches	x, inches	y, inches
0.0000	0.0000	3.1759	1.7062
0.0005	0.0171	3.9360	1.6370
0.0199	0.1224	4.8058	1.5298
0.0641	0.2387	5.7561	1.4009
0.1322	0.3625	6.7611	1.2594
0.2234	0.4913	8.3167	1.0386
0.3370	0.6229	9.8563	0.8225
0.4727	0.7553		
0.6295	0.8868	11.3002	0.6227
0.8069	1.0154	11.7475	0.5604
1.0040	1.1395	12.9526	0.3907
1.2200	1.2572	13.9103	0.2459
1.4538	1.3670	14.3900	0.1633
1.9705	1.5543	14.7328	0.0923
2.5439	1.6826	14.9341	0.0347
		15.0000	0.0000

Lower Surface

x, inches	y, inches	x, inches	y, inches
0.0000	0.0000	6.1216	-0.0935
0.0096	-0.0715	7.2337	-0.0190
0.0561	-0.1479	8.3585	0.0436
0.1396	-0.2207	9.4696	0.0904
0.2525	-0.2882	10.5402	0.1190
0.3920	-0.3476	11.5443	0.1289
0.5567	-0.3921	12.4569	0.1213
0.7544	-0.4165	13.2551	0.0995
0.9909	-0.4273	13.9190	0.0685
1.2633	-0.4289	14.4318	0.0353
1.5700	-0.4218	14.7810	0.0103
2.2797	-0.3863	15.0000	0.0000
3.1068	-0.3282		
4.0356	-0.2550		
5.0477	-0.1743		
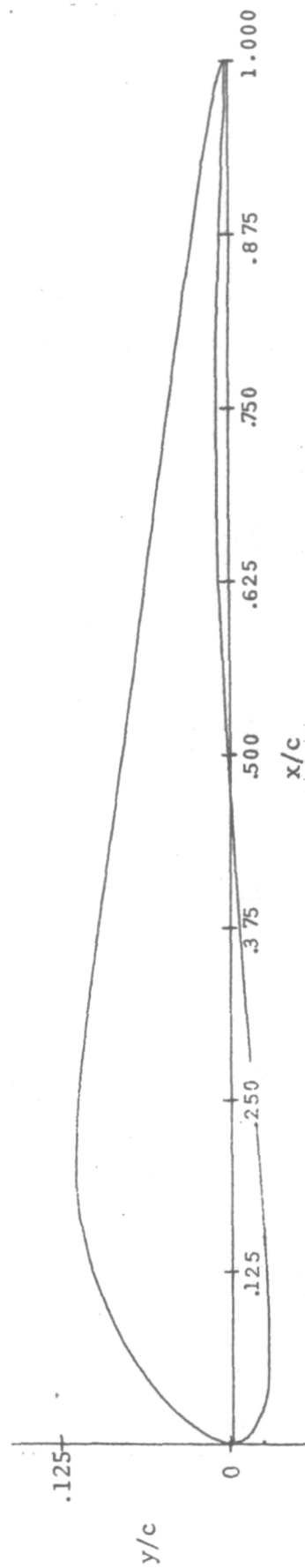
Figure 1. UI-1720 Airfoil Contour and Coordinates
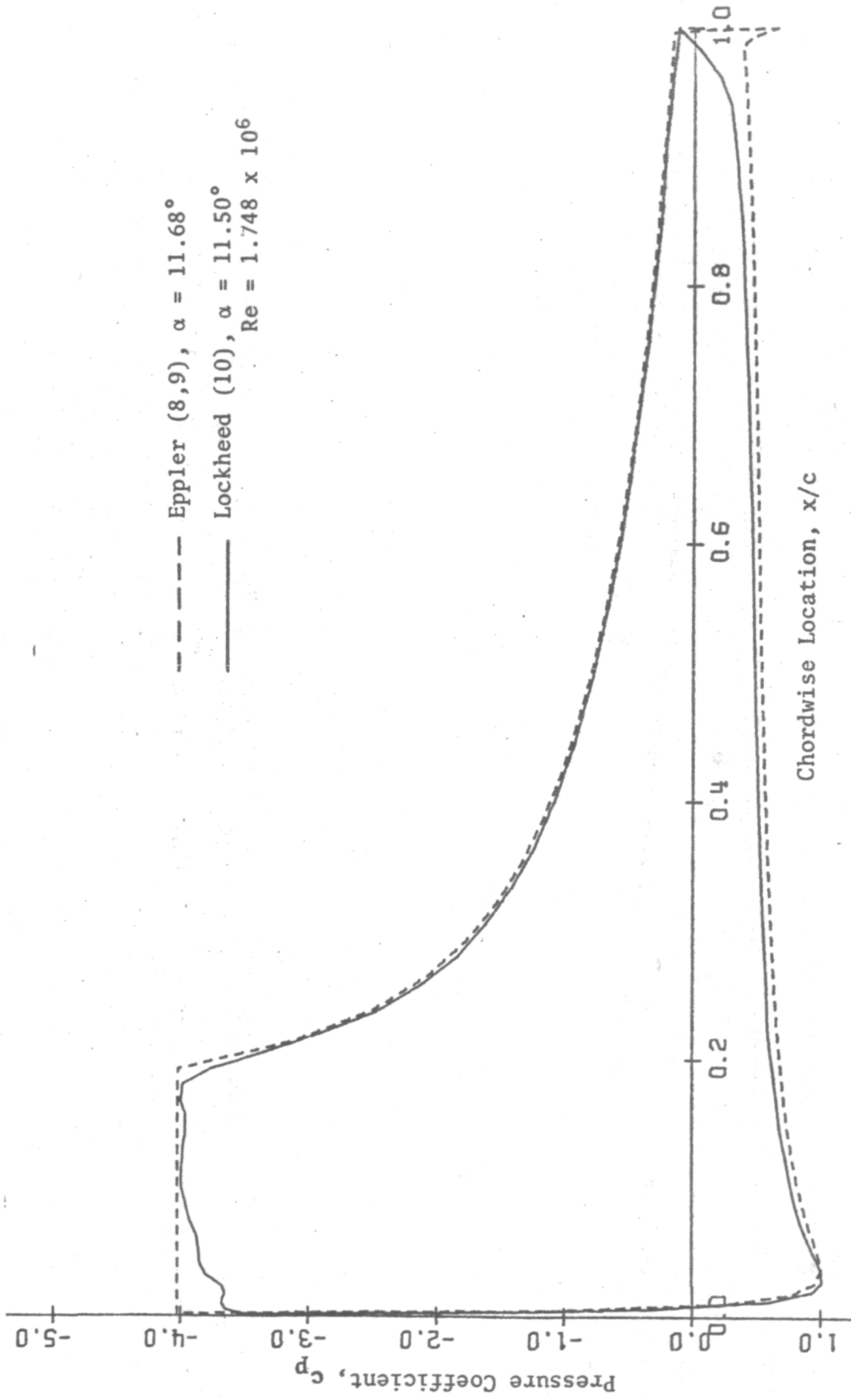
Figure 2. Theoretical Pressure Distributions for the UI-1720 Airfoil
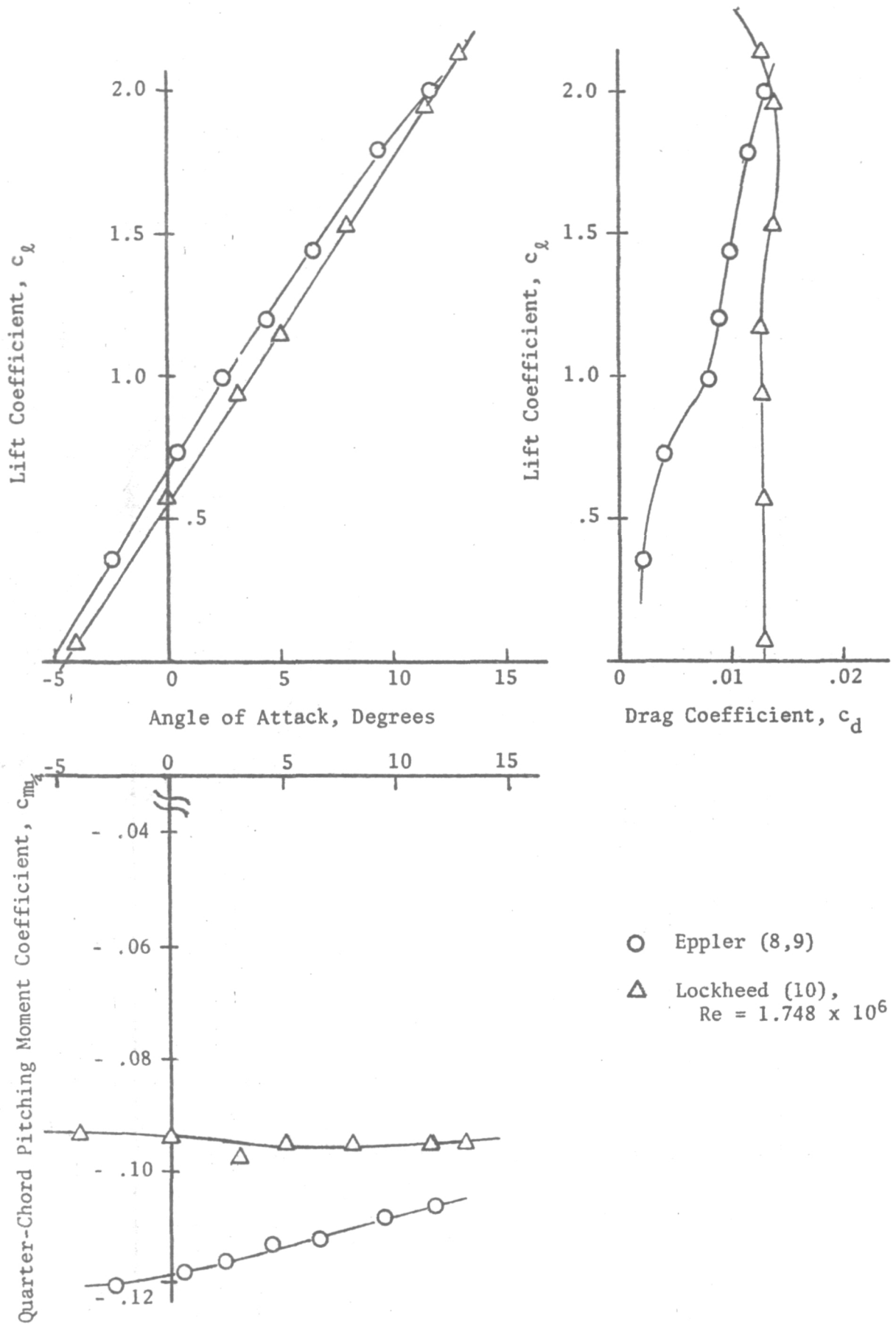
Figure 3. Theoretical Sectional Characteristics

31"

153"

60"

10"

60"

60"

30"

17½"

175"

40.2'

Flow

Top View

60"

Contraction

Test Section

Diffuser

Settling Section

Screens and Honeycomb

Diffuser-Transition

Fan
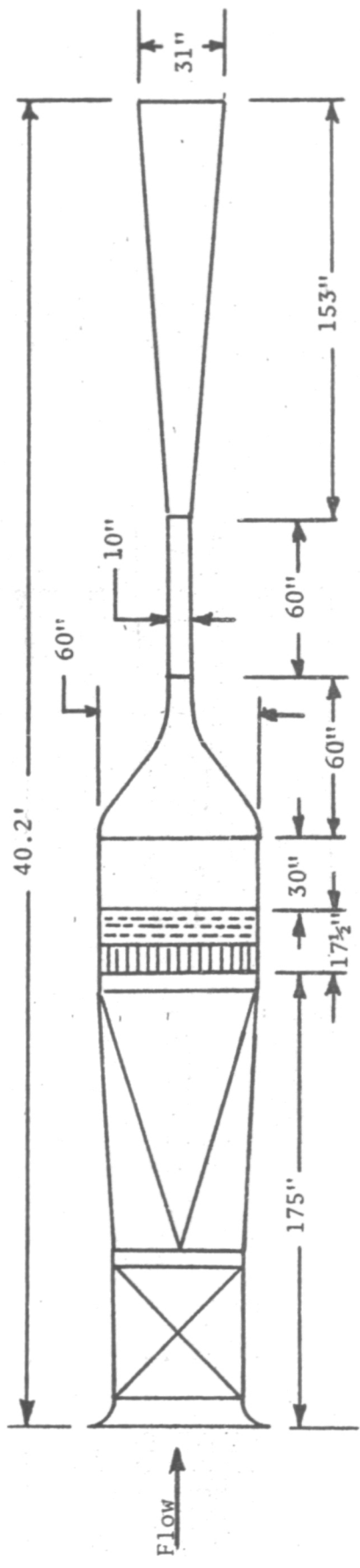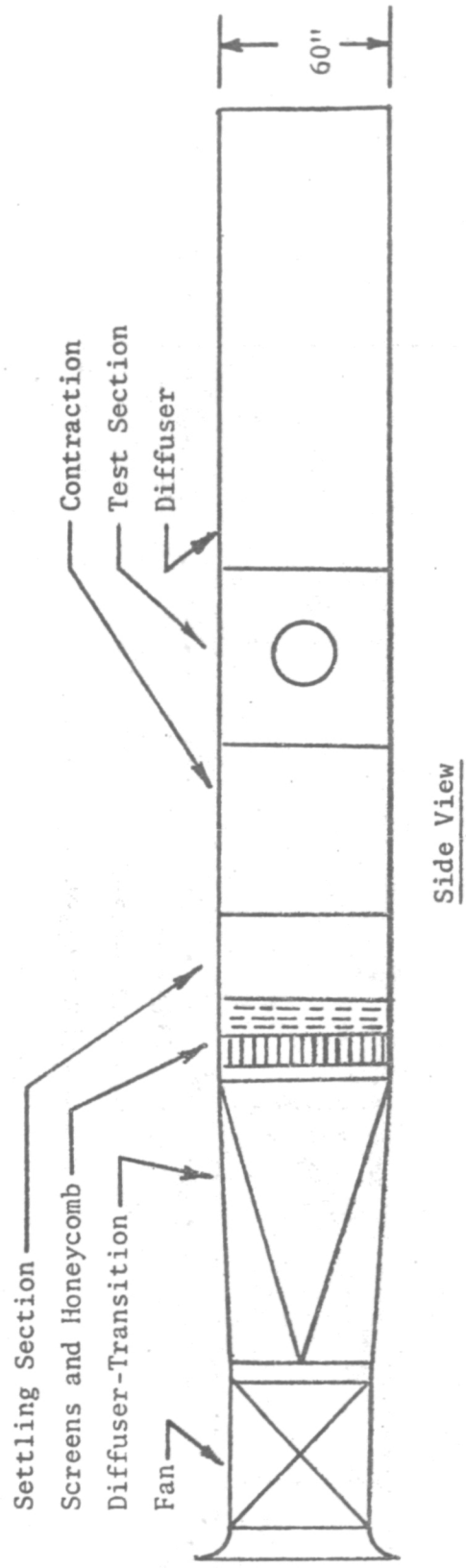
Side View

Figure 4. Layout of the University of Illinois Two-Dimensional, Low-Speed Wind Tunnel
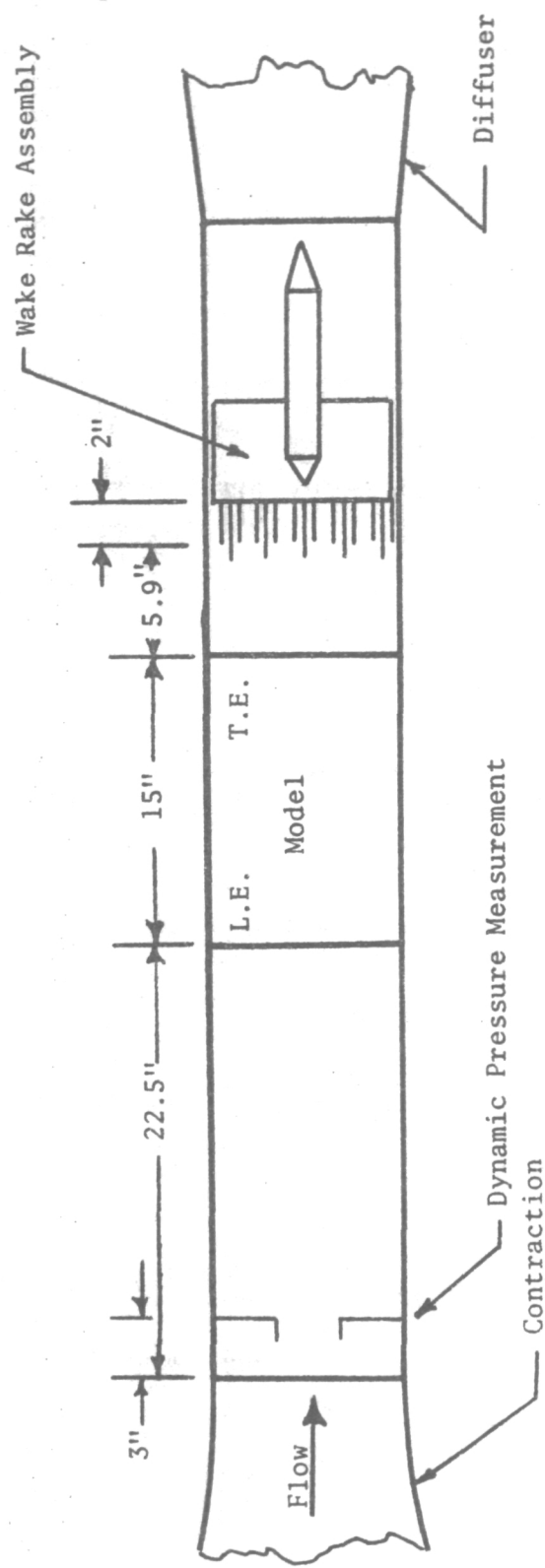
Figure 5. Test Section Layout (Top View)
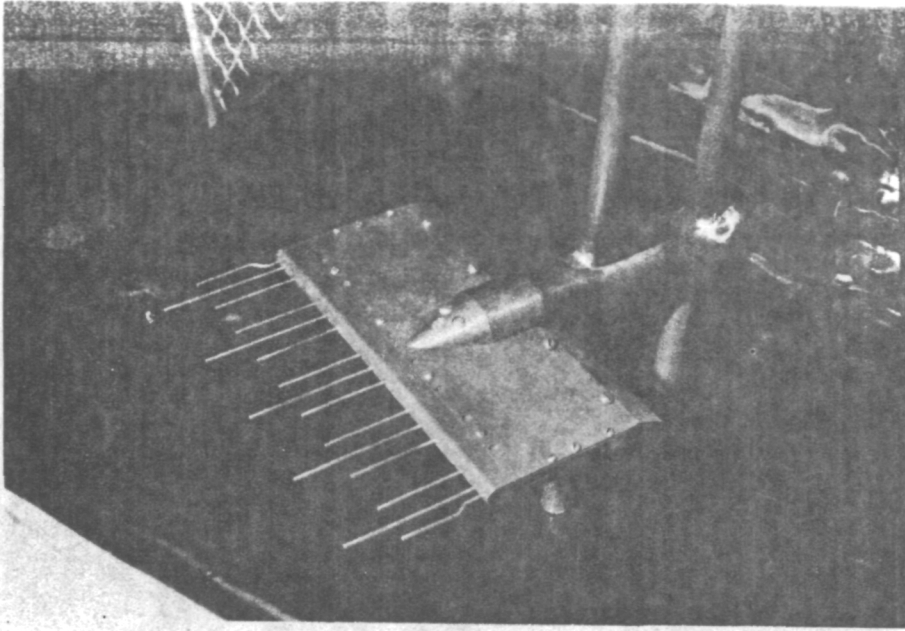
a. Photograph of Wake Rake
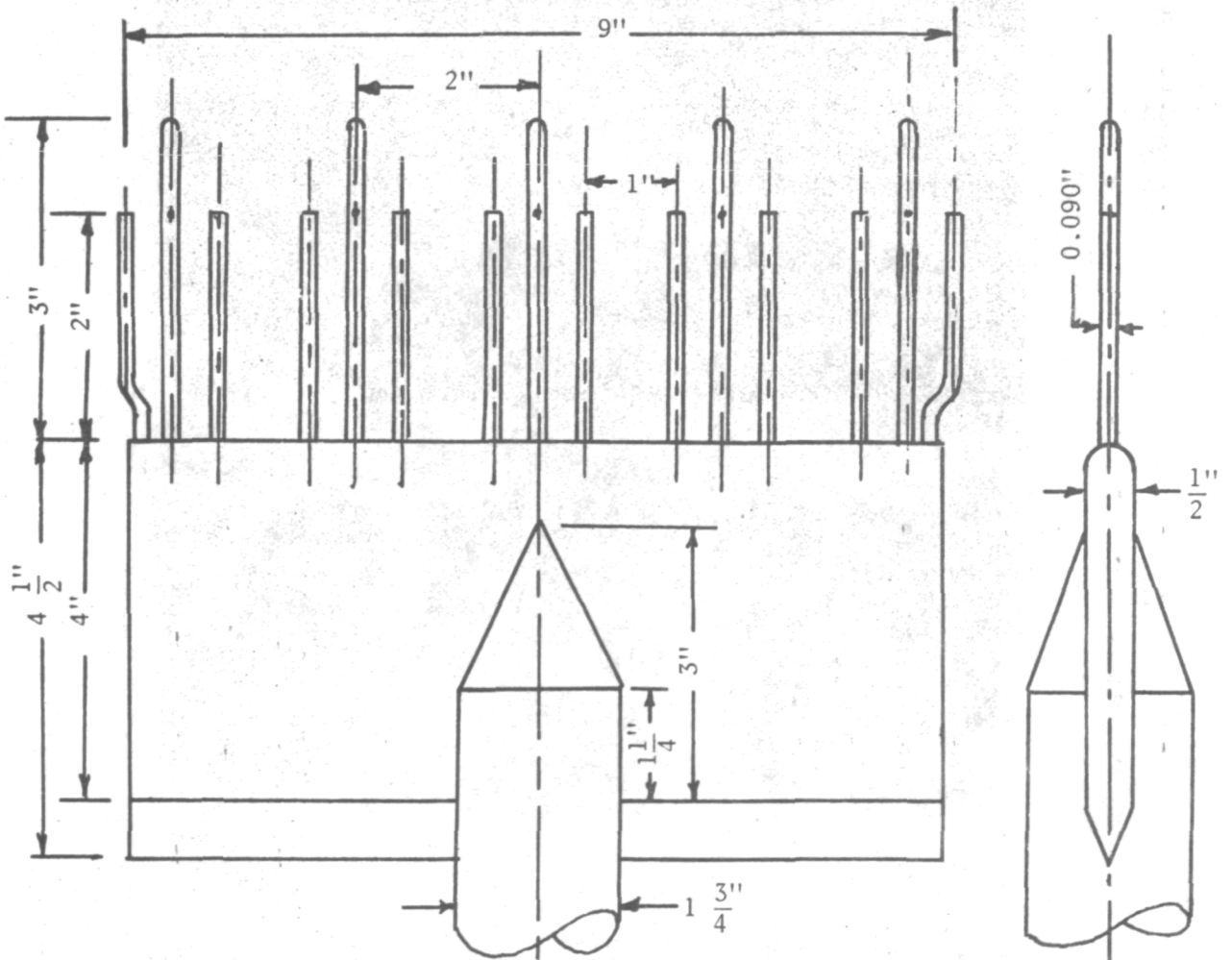
b. Layout of Wake Rake

Figure 6. Wake Rake Details
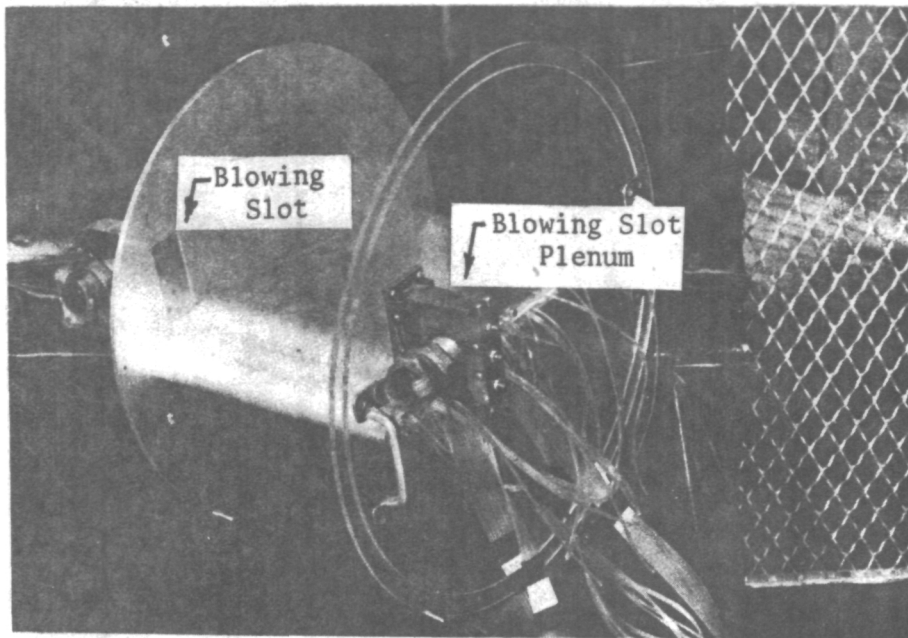
a. Wing Model Assembly
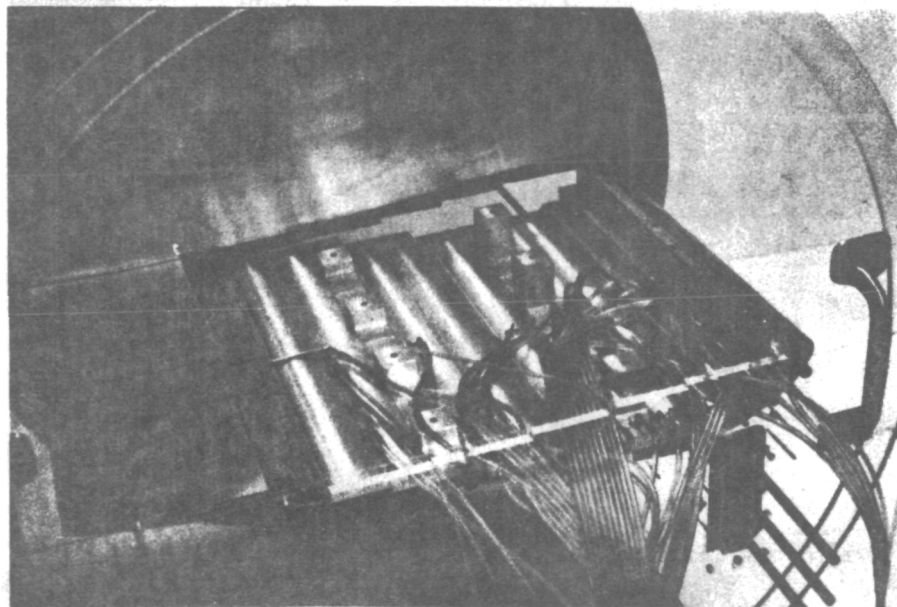
b. Lower Plate Removed Showing Pressure Leads Inside Model

Figure 7. Model Wing Photographs

Inner Surface
of Endplate

Slot

Air Supply
Inlet Hole

Plenum

Rods for Adjusting
Slot Opening
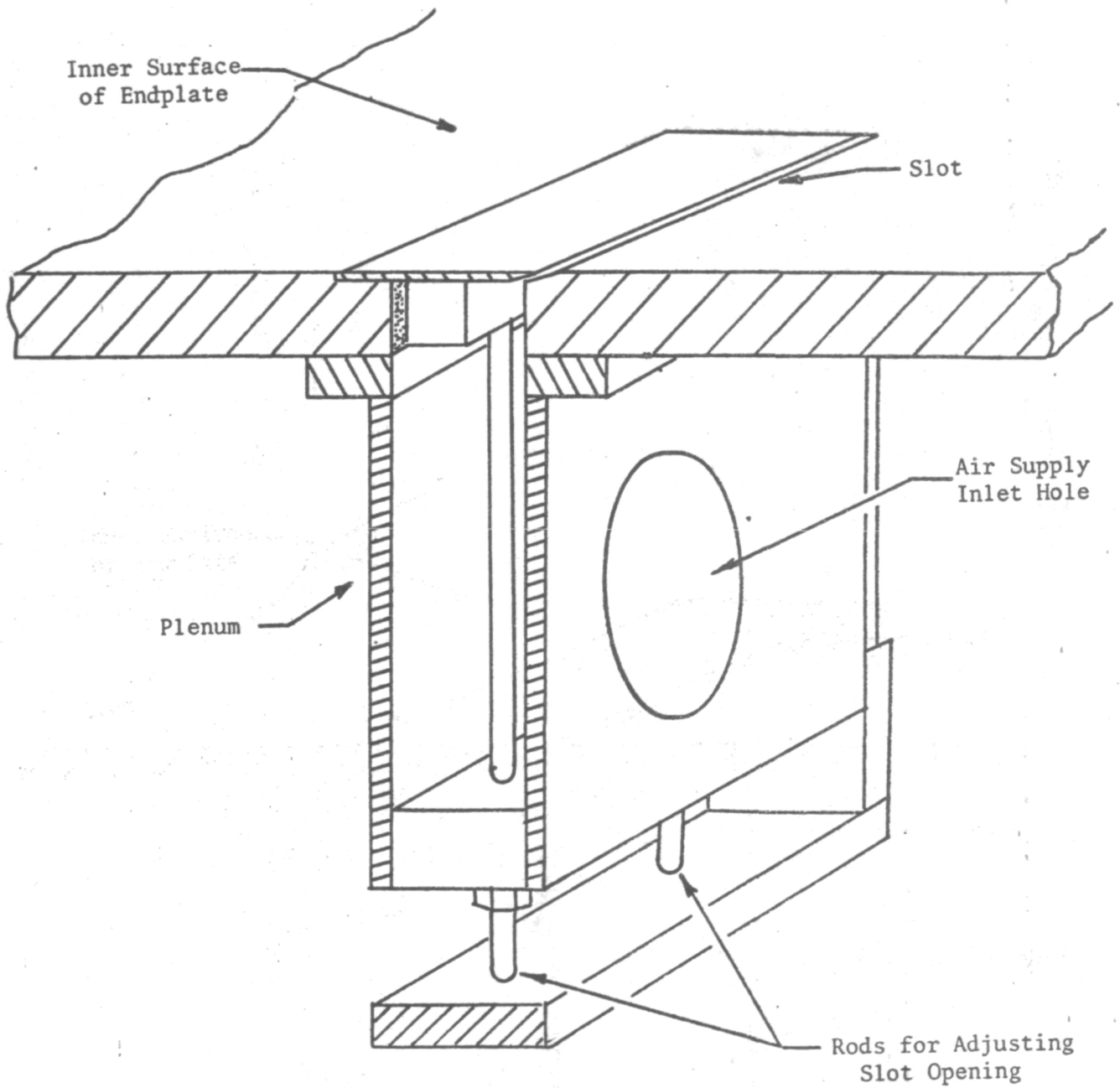
Figure 8. Sectional Sketch of Blowing Slot Assembly
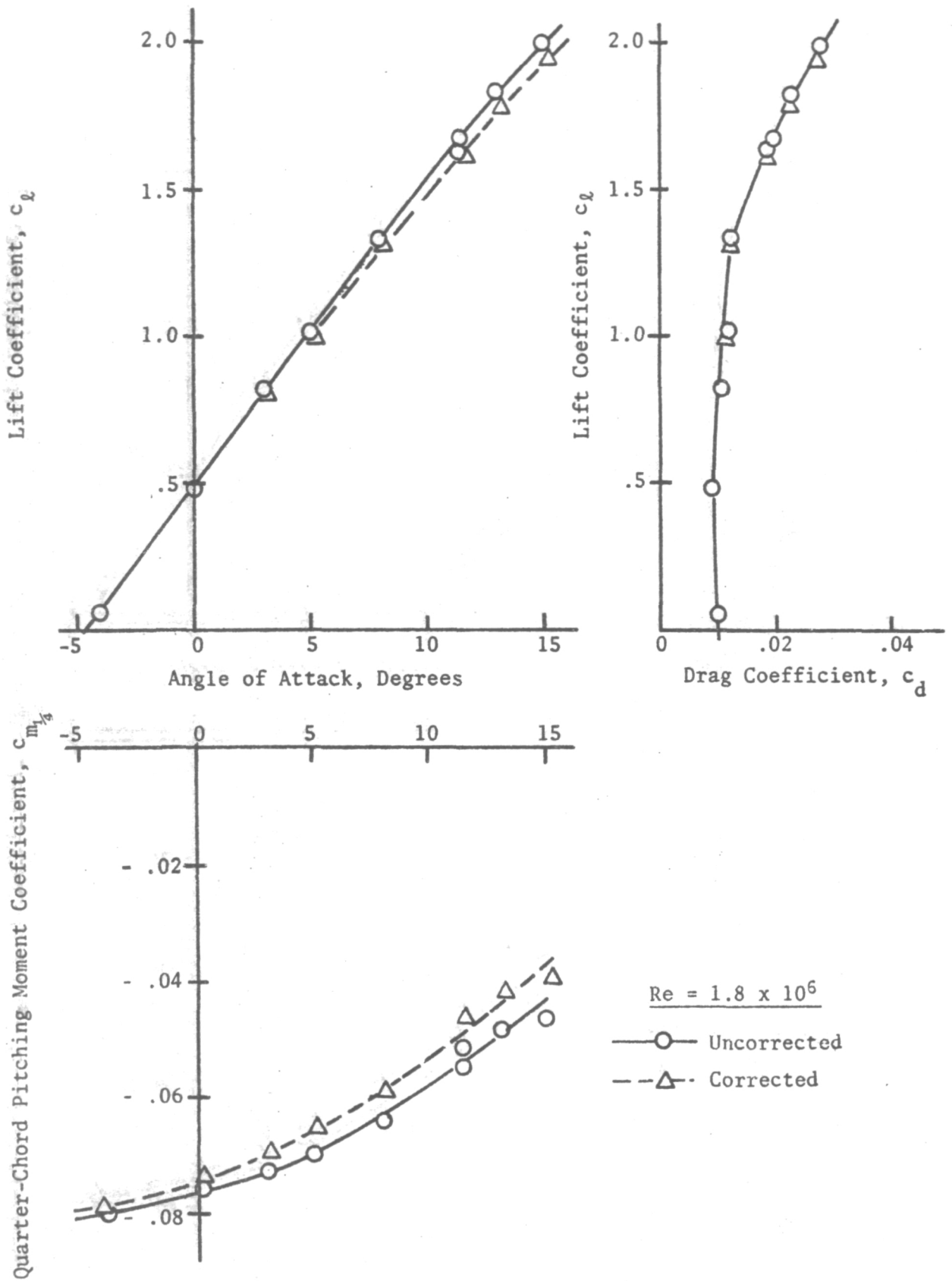
Figure 9. Effect of Tunnel Boundary Corrections
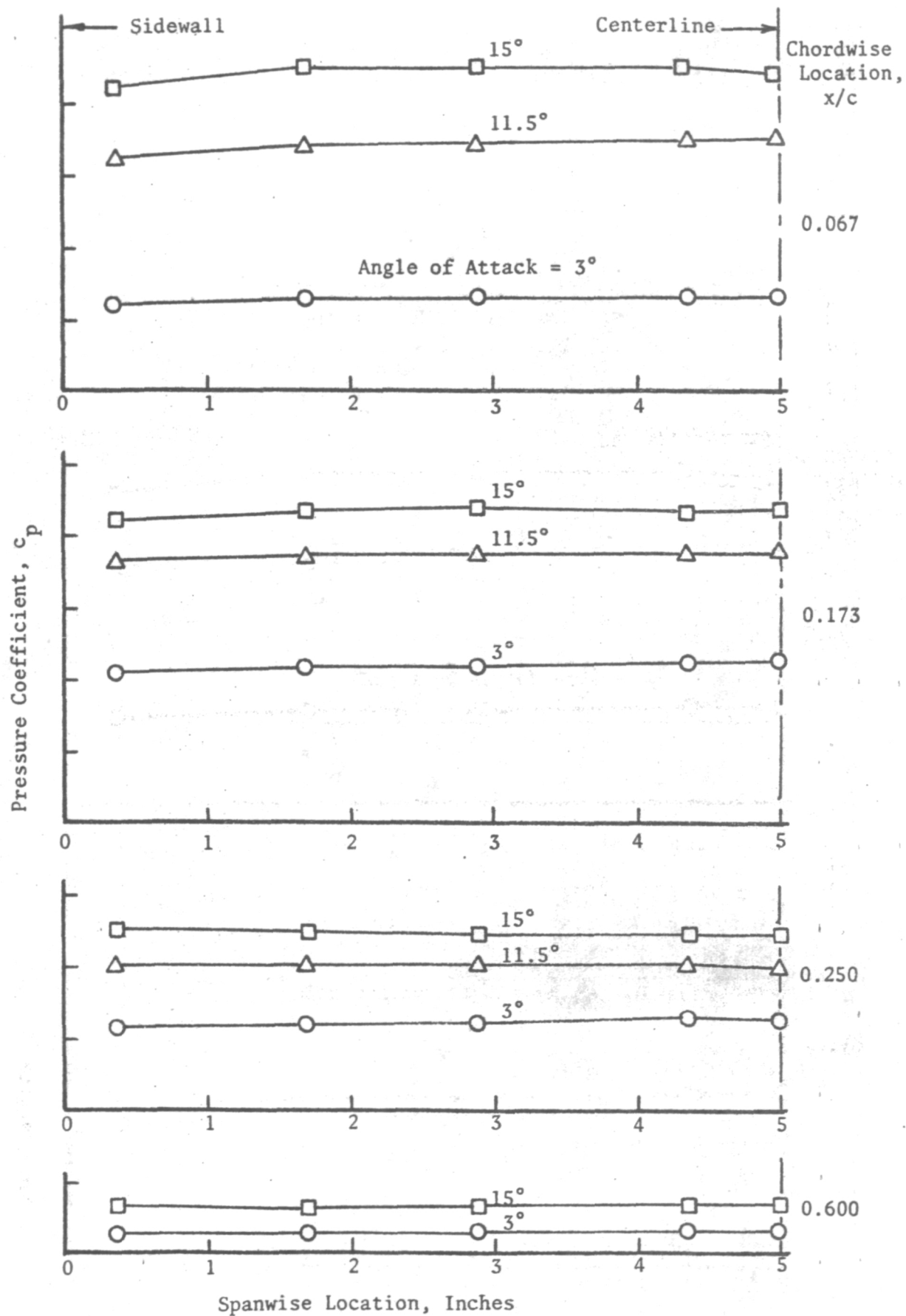
Figure 10. Spanwise Pressure Distributions; Re = 1.8 x 10^6
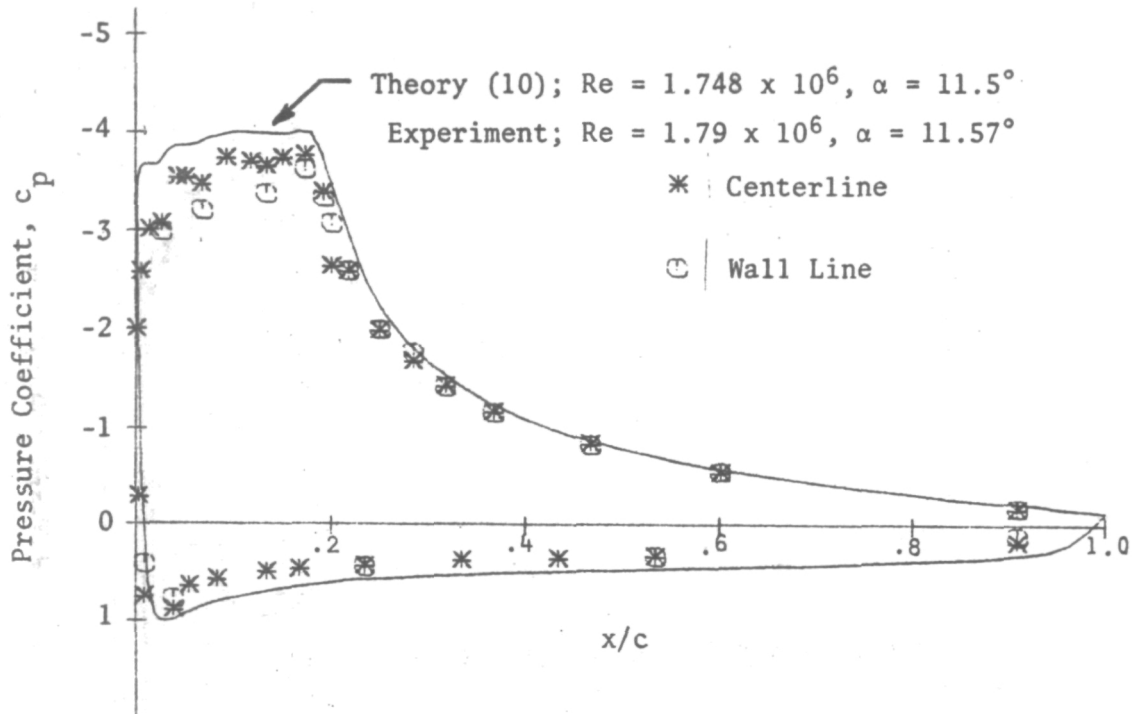
Figure 11. Comparison of Centerline and Wall Line Pressure Distributions

$Re = 1.40 \times 10^6$

$\alpha = 11.67°$
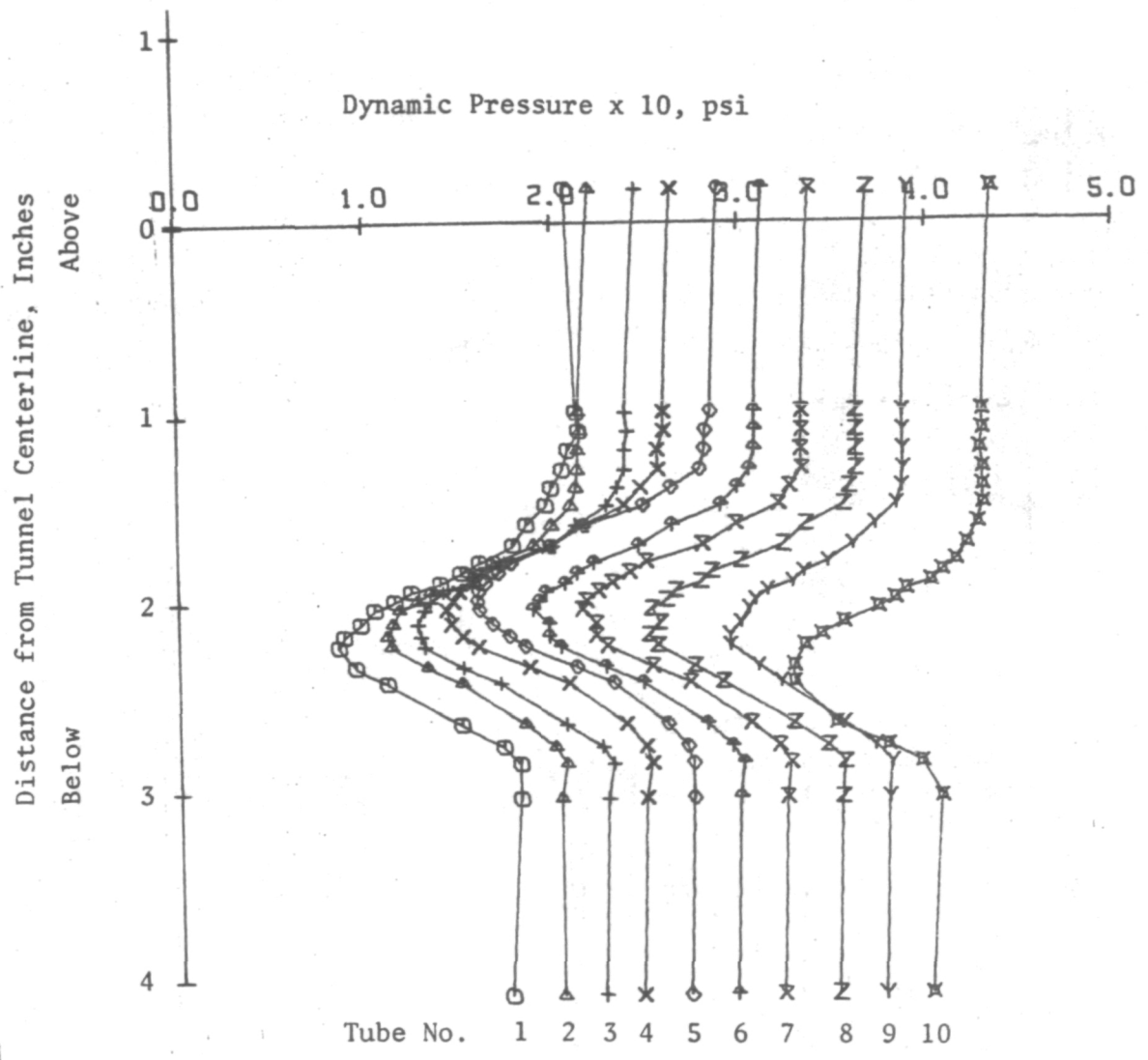
Figure 12. Dynamic Pressure Distribution in the Wake
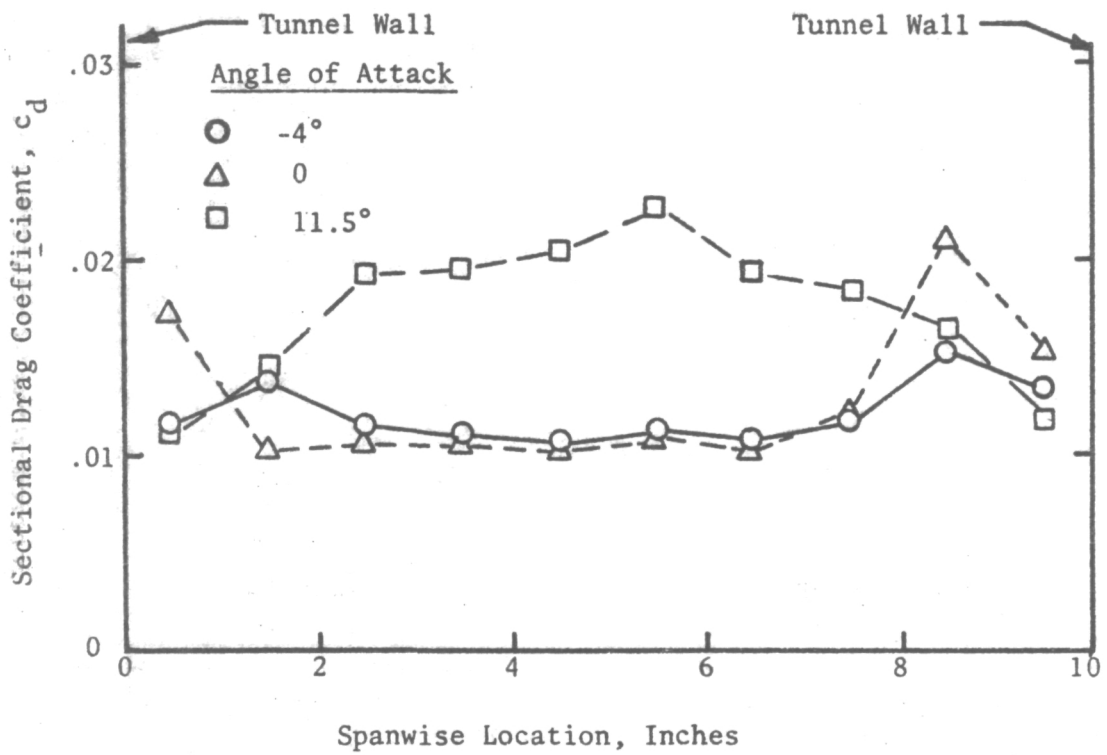
Figure 13. Spanwise Distribution of Drag Coefficient
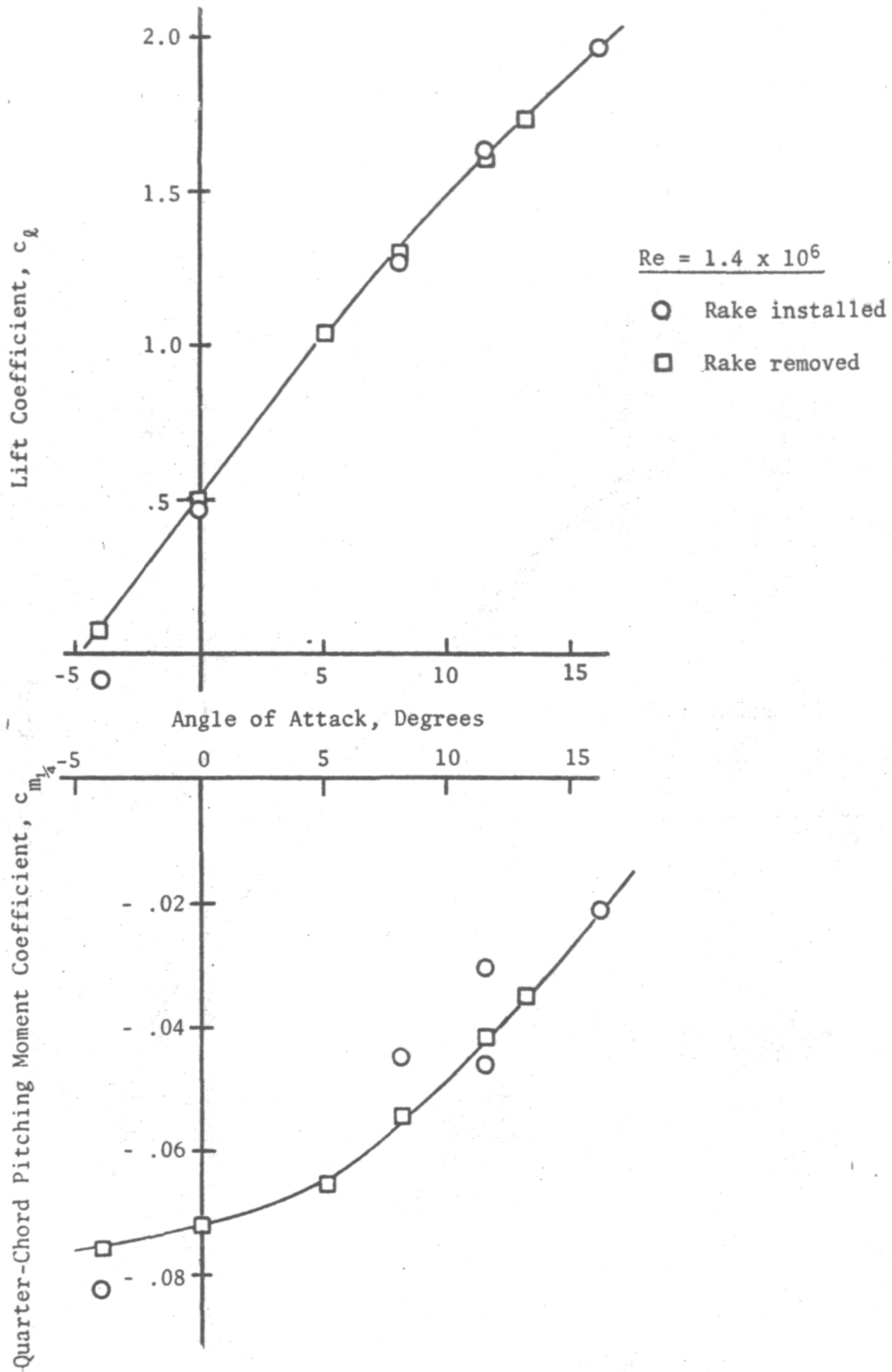
Figure 14.   Effect of Wake Rake
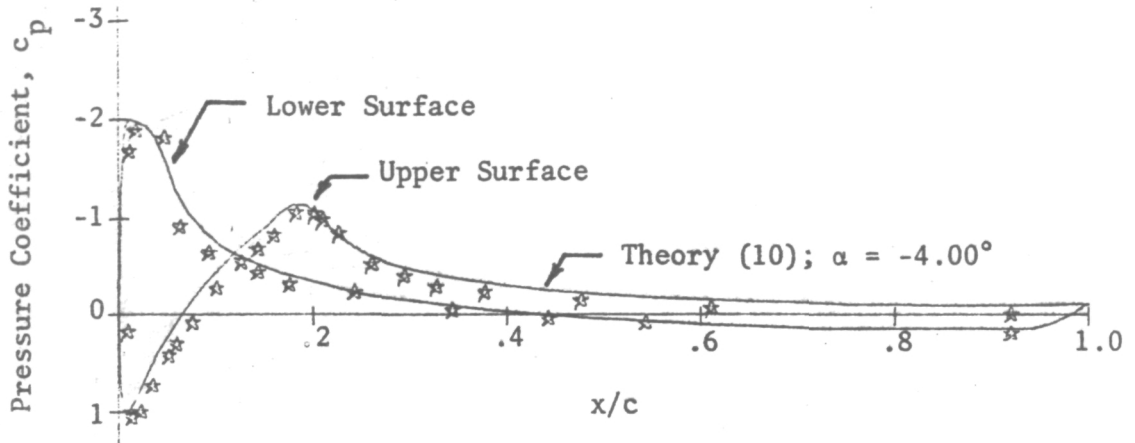
a. $\alpha = -4.13°$
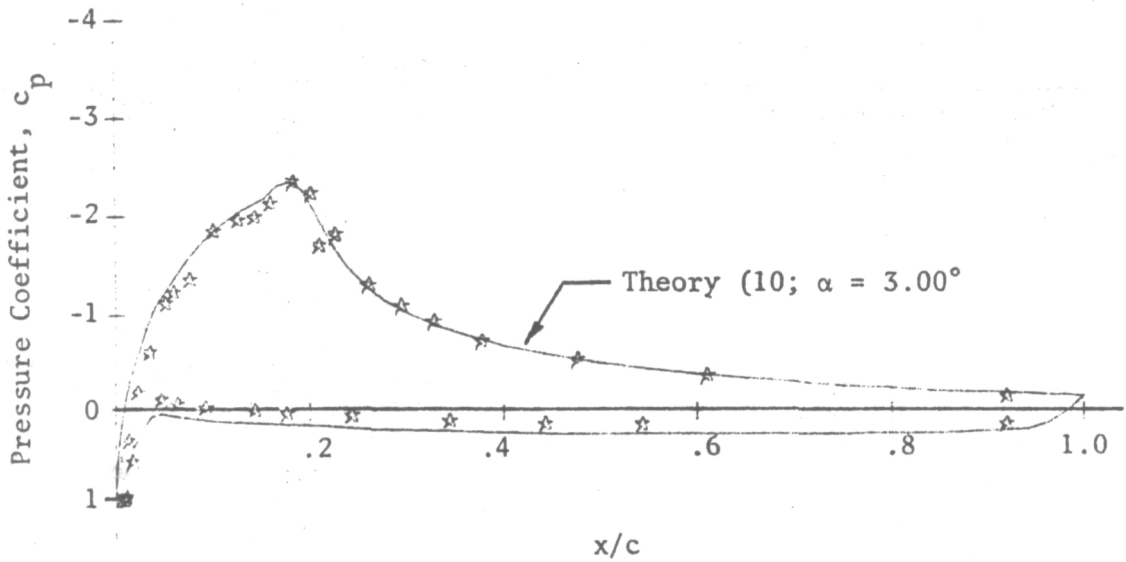
b. $\alpha = 3.06°$

Figure 15. Chordwise Pressure Distributions at Re - 1.8 x 10^6

c. α = 11.57°
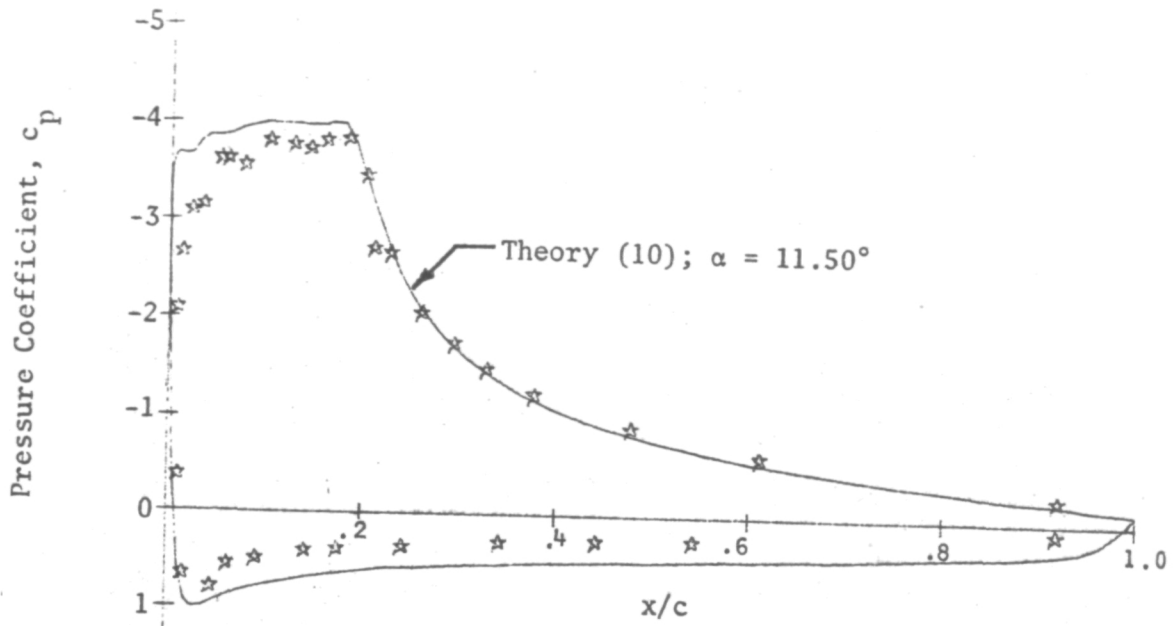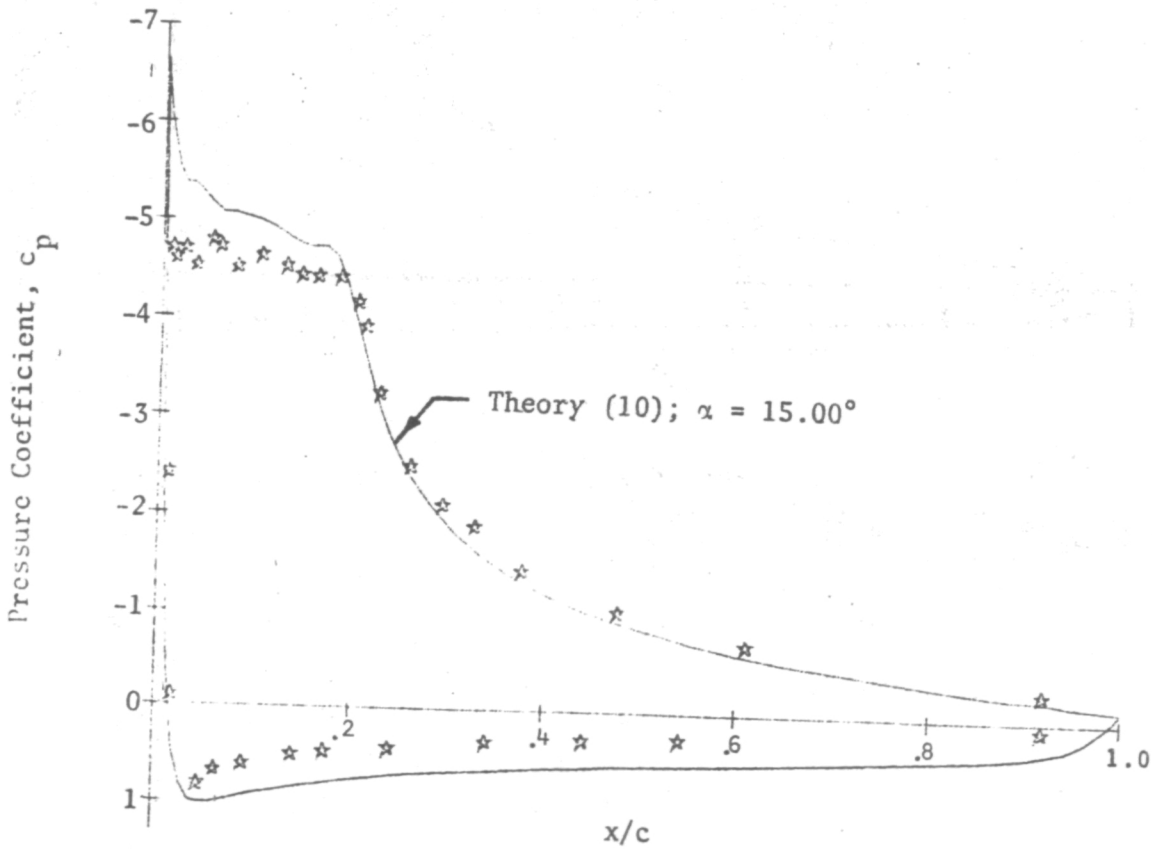
d. α = 15.21°

Figure 15.   Concluded
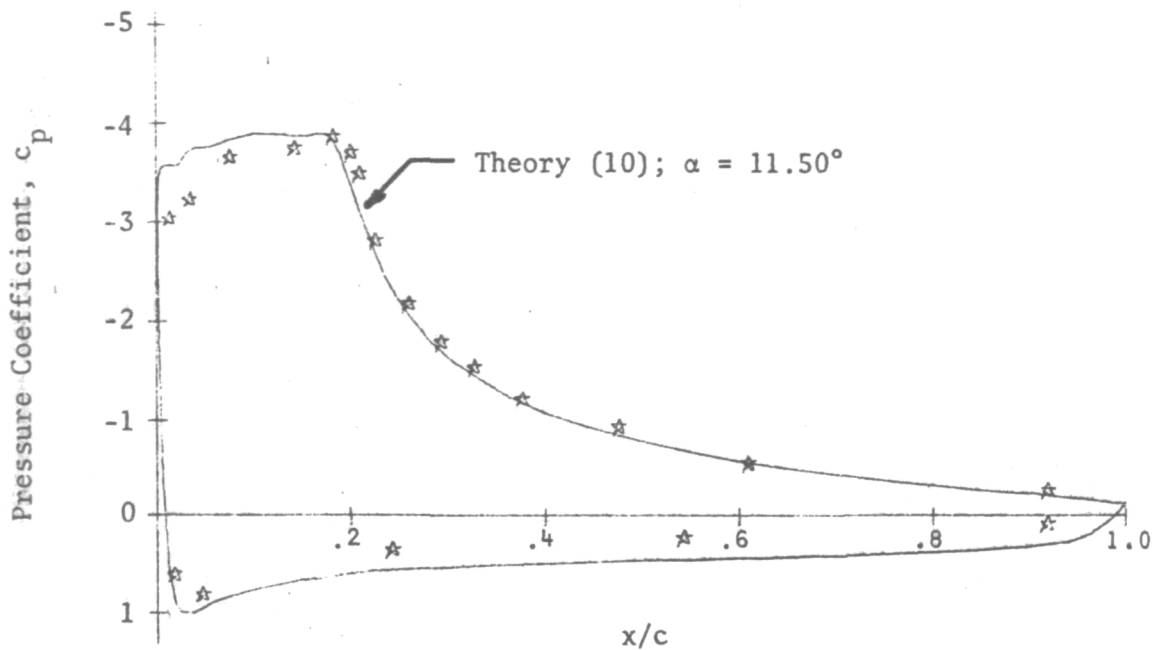
a. $\alpha = 11.67°$
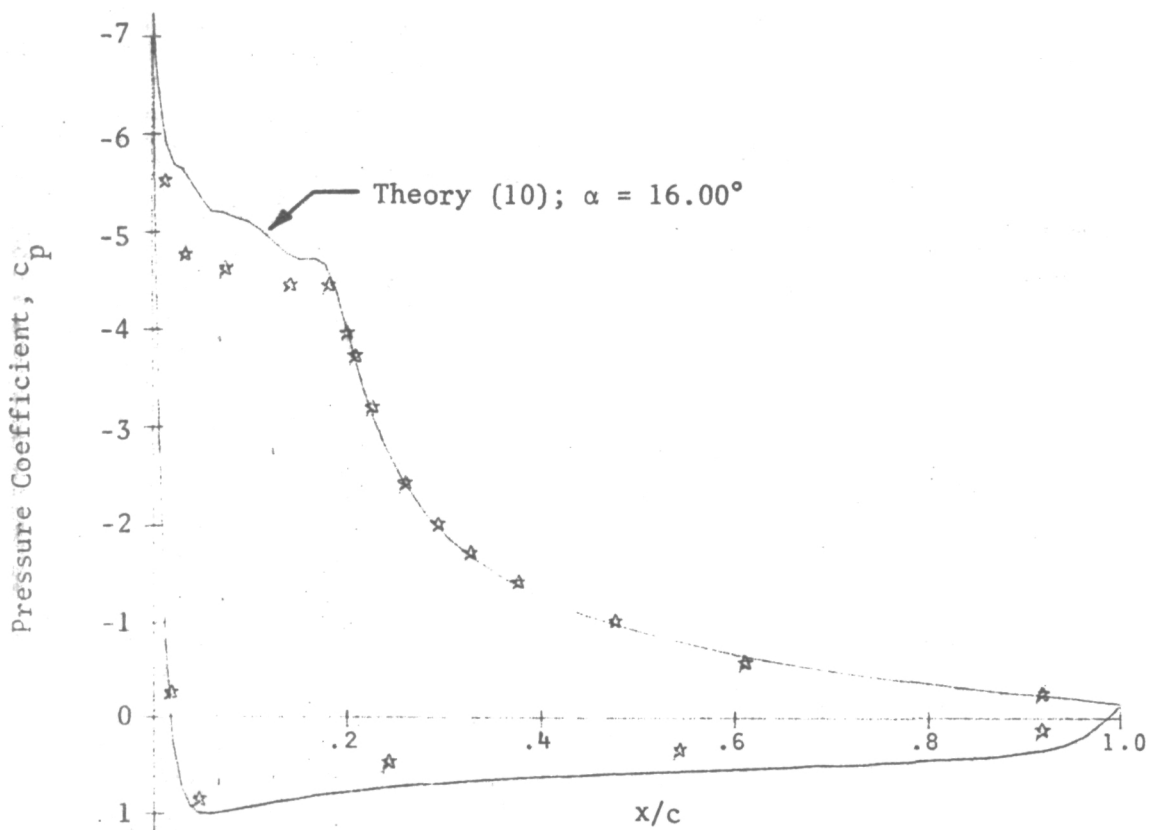
b. $\alpha = 16.22°$

Figure 16. Chordwise Pressure Distributions at Re = 1.4 x 10^{6}
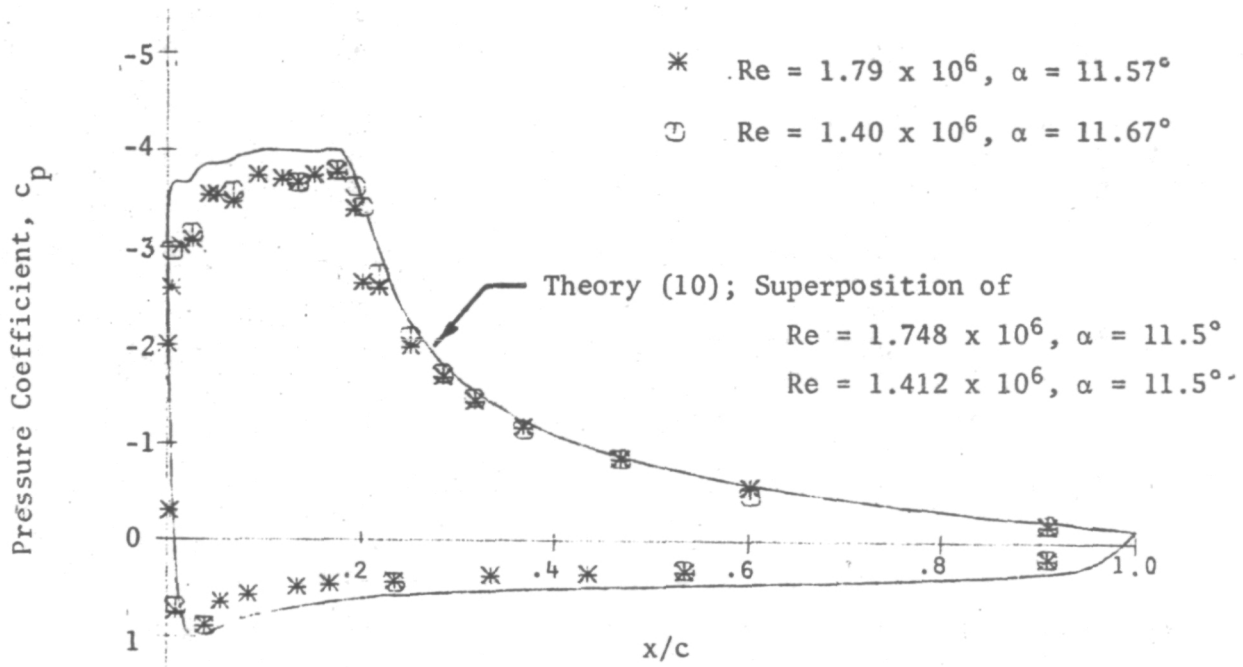
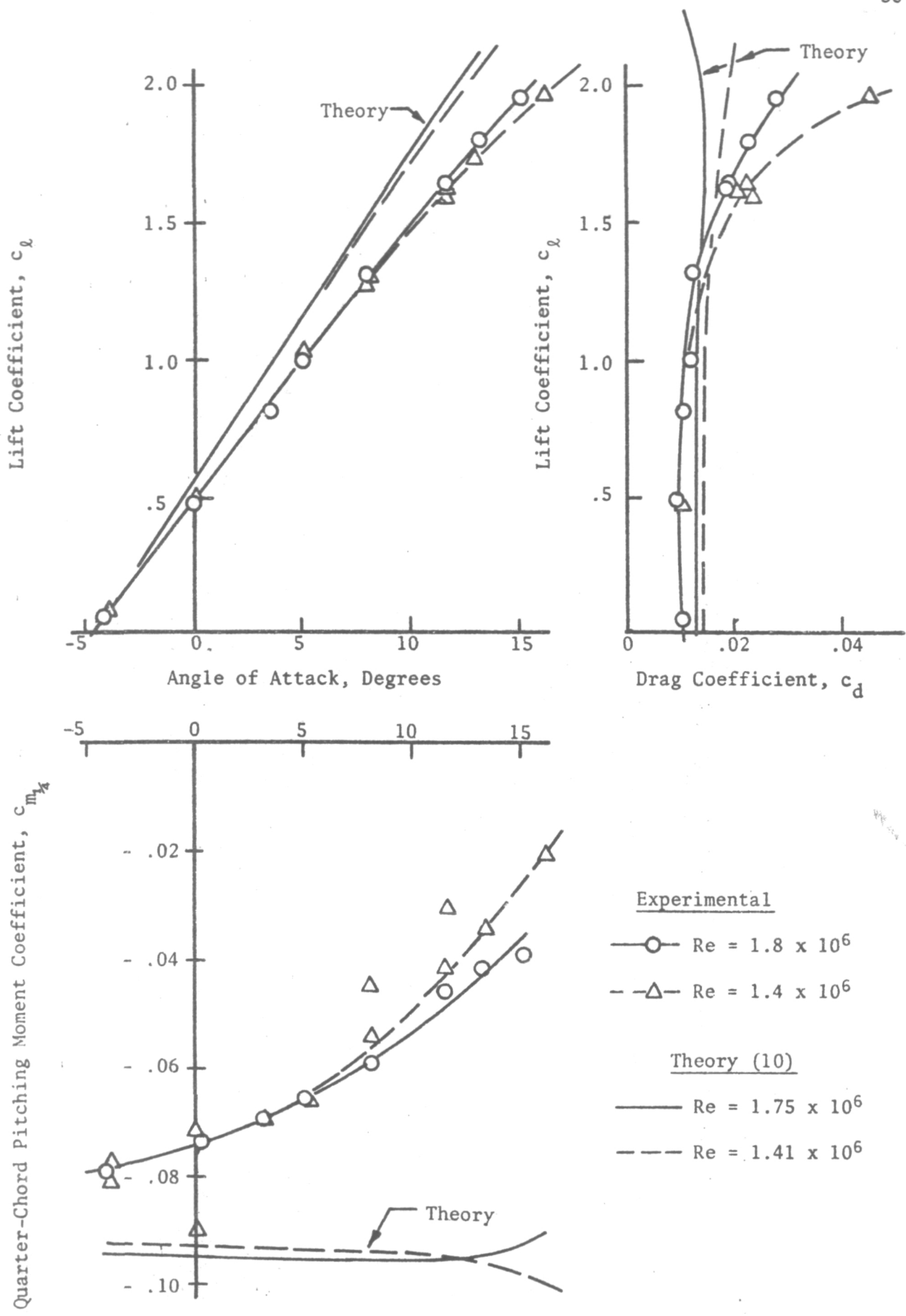Figure 17. Effect of Reynolds Number on Pressure Distribution

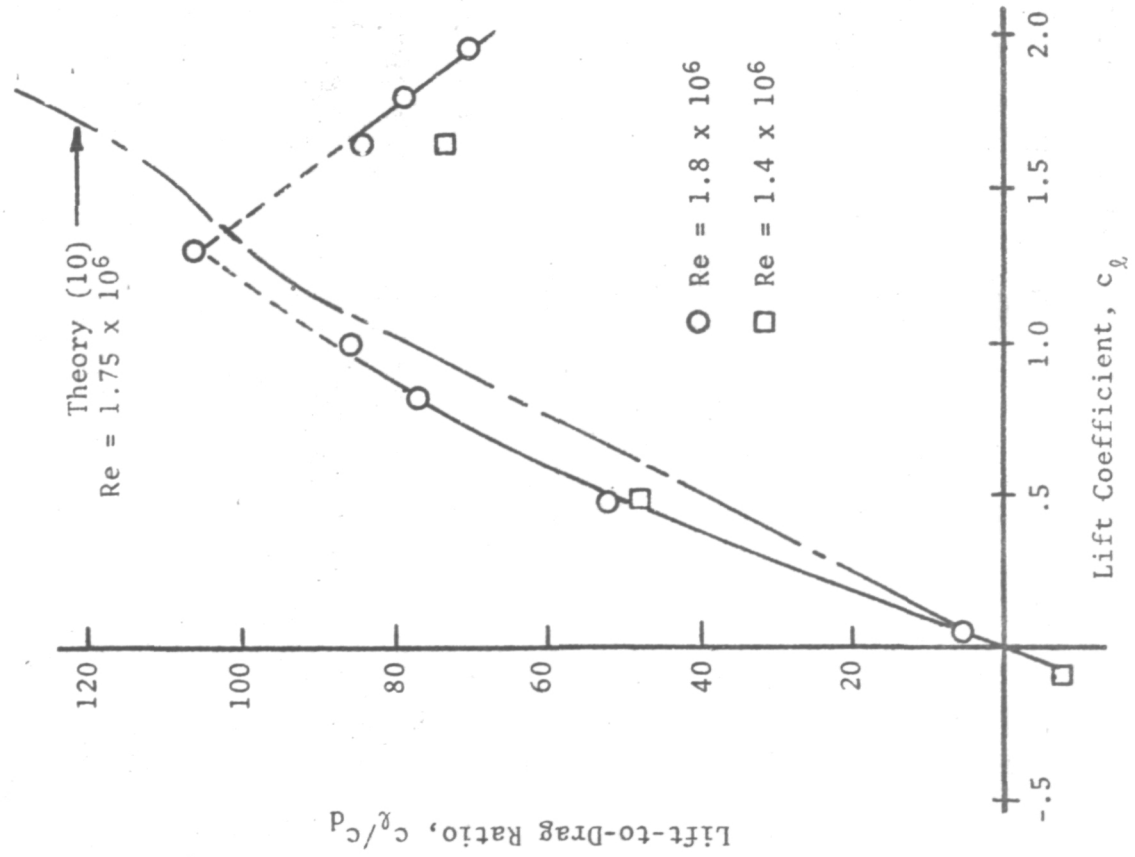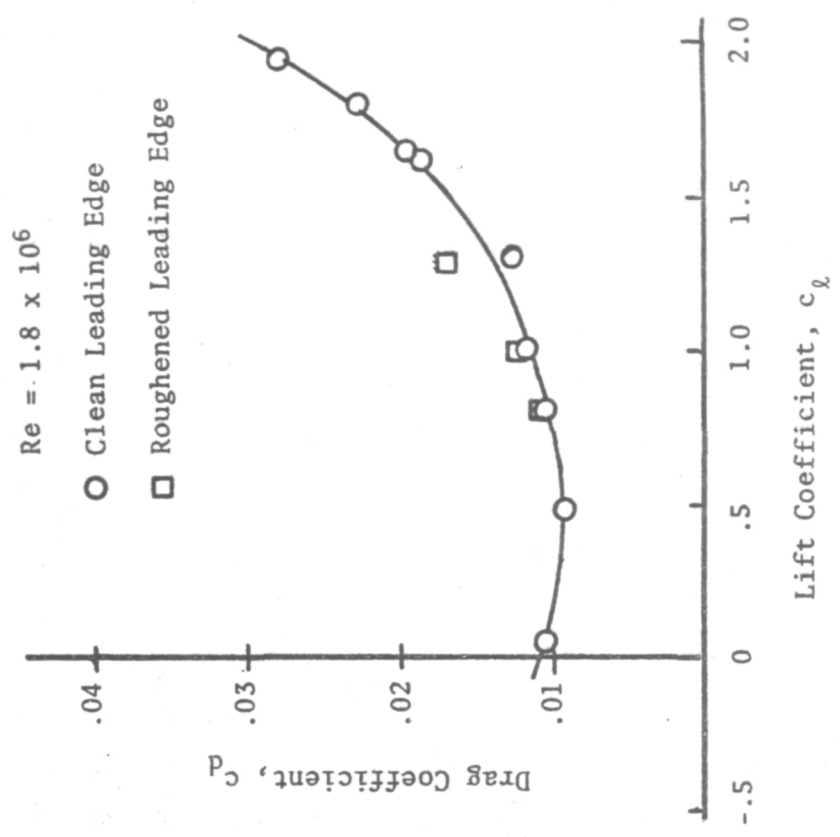Figure 18. Sectional Characteristics of the !!!-1/?? Airfoil

Figure 20. Effect of Leading-Edge Roughness on Drag

Figure 19. Lift-to-Drag Ratio